2018-1289

AIAA Aerospace Sciences Meeting, 8–12 January 2018, Kissimmee, Florida.

Classifying Exotic Wakes with a Flow Speed Sensor

Mengying Wang* and Maziar S. Hemati†

Marine swimmers are able to detect external flow structures and exploit them to reduce locomotive effort. To achieve this advantage, these swimmers use mechanosensory organs to sense their hydrodynamic surroundings. An ability to sense and classify nearby wakes can lead to enhanced control and decision making in the context of bioinspired robotic swimmers and underwater vehicles. In previous work, we used an ideal flow model to demonstrate the viability of detecting and classifying vortex wakes from hydrodynamic sensor measurements. In the present study, we extend our previous wake detection protocol to enable online wake classification from streams of hydrodynamic sensor measurements. The streaming protocol is developed using short-time Fourier analysis and supervised learning algorithms. The online wake detection protocol is found to exhibit a comparable rate of classification accuracy as the original protocol. The online protocol's performance is also assessed in the face of synthetic measurement noise of various intensities. Noisy measurements degrade the classification accuracy in many cases, but performance can be improved through proper protocol design and tuning.

Nomenclature

c	chord length
$\mathrm{d}t$	convective time step
h	lateral separation of body and wake
L	length of periodic wake strip
γ	vortex strength ratio
$\mathcal{Q} + i\mathcal{P}$	linear impulse
T_o	sliding window overlap time
T_s	full sliding duration
T_w	window duration
U'	tangential velocity at the collocation point
U_∞	uniform flow velocity
U_{wake}	vortex wake induced velocity
V	feature vector
X	normalized horizontal distance between vortices
Y	normalized vertical distance between vortices
(μ, a, σ)	bell curve parameters
Γ^{panel}	panel strength

I. Introduction

Many marine swimmers are able to interact with nearby wake vortices to save energy as they propel themselves through their fluid environment.[1,2] To achieve this advantage, marine swimmers utilize mechanosensory organs, such as the lateral line system, to sense hydrodynamic signals and detect vortical

*Research Assistant, Department of Aerospace Engineering and Mechanics, Member AIAA, wang5772@umn.edu

†Assistant Professor, Department of Aerospace Engineering and Mechanics, Senior Member AIAA, mhemati@umn.edu.

Copyright © 2018 by Mengying Wang and Maziar S. Hemati. Published by the American Institute of Aeronautics and Astronautics, Inc. with permission.

flow structures. In the context of robotic swimmers and underwater vehicles, an ability to sense, detect, and classify nearby wakes provides an opportunity for enhanced situational awareness. Some past studies have demonstrated closed-loop locomotion control in the presence of wakes, leveraging model-based estimation to reconstruct the state of the fluid from sensor measurements.[3] These model-based strategies have primarily focused on operation in von Kármán-type wakes, which poses a practical problem since many other wake types also exist. If a more exotic wake type is encountered, then the model-based estimation and control laws would prove unsatisfactory at best. Thus, one of our primary motivations for studying wake detection and classification is to establish a path toward multi-model approaches for locomotion control.

In a recent study, we formulated a general framework for wake detection and classification.[4] The protocol was established as a supervised learning problem, in which a wake classification library was first constructed, then used to classify unknown wake types from time-series measurements of velocity at a single point on a body. The framework was demonstrated on an ideal flow model in a simple proof-of-concept setting, and was found to yield an accuracy rate of 95% over a wide range of algorithmic parameters. However, in that study, we assumed full access to the complete set of time-series measurements acquired over many convective times. In the present study, we will extend the classification protocol to accommodate streams of sensor measurements in an online fashion. In particular, we formulate the "feature extraction" stage of the supervised learning algorithm in terms of a sliding window, which has demonstrable sensor-noise handling qualities as well. Further, the new streaming protocol allows detection and classification in a time-varying/non-stationary environment, making the framework more relevant for practical use.

In Section II, we summarize the original wake detection protocol and formulate the streaming feature extraction concept. In Section III, we describe the idealized flow model used to simulate the hydrodynamic signatures imparted by various wakes on a fish-like body. The results of the streaming wake detection protocol are reported in Section IV. Finally, discuss the results and draw conclusions in Section V.

II. Wake Classification Protocol

Associating measured hydrodynamic signals with a particular wake type is the main goal we want to achieve to approach the wake type detection problem. First, we build a library of wake signatures and associate every entry of the library with its wake type. After constructing the library, we use a supervised learning strategy to classify an unknown wake by comparing its hydrodynamic signals with the entries in the library. The synthesis of this protocol is following our previous work,[4] which is summarized graphically in Fig. 1. Unlike our previous work with the full access to the sensor measurement before proceeding the algorithm, in this study, we will extend our method to deal with real-time signals. This method will benefit to save the waiting time for data collection and also detect the changes happened in datastreams such that we can notice the appearance of the oncoming wake from the measurements.

To construct a wake classification library, we obtain sensor measurements from multiple realizations from each of various wake types. The number of realizations r is sufficiently large so as to guarantee the richness of the library. Because the sensor measurements are collected as time series data, care must be taken to develop a method that is invariant to the start time of data collection. Here, a "static" feature vector V_i is extracted from the data by first transforming the time-domain signal into the frequency domain, then summarizing each signature with three parameters that define a bell curve fit to this signature in frequency space. In our previous work, we showed that this feature vector provided a convenient and relatively robust summary of the time-series signature imparted by various idealized wakes in our flow model.[4] In that study, we used the fast Fourier transform to extract the frequency content of the time-domain signal from each of the r wake realizations used to build-up the library $\{V_1, V_2, \ldots, V_r\}$, as shown in Fig. 1a. Here, as the library is constructed, we assume that the wake-type associated with each feature is known. In the event that the wake type is unknown during the library construction stage, then an unsupervised wake regime learning strategy can be devised to group and label wakes according to similarities in their dynamics.[8]

Once the library is constructed, we can proceed to classify unknown wakes by comparing against entries in the library. To do so, the measured time-series signal is converted into a static feature vector V_{test}, then compared against entries in the library to determine the "closest match" and the most likely classification of the unknown wake type (see Fig. 1b). A variety of supervised learning algorithms can be applied for the classification task. In our study, we use the k-nearest-neighbor (KNN) algorithm owing to its simplicity.[9,10] Using this approach, a classification accuracy rate of 95% can be attained for a wide range of algorithm parameter values.[4]

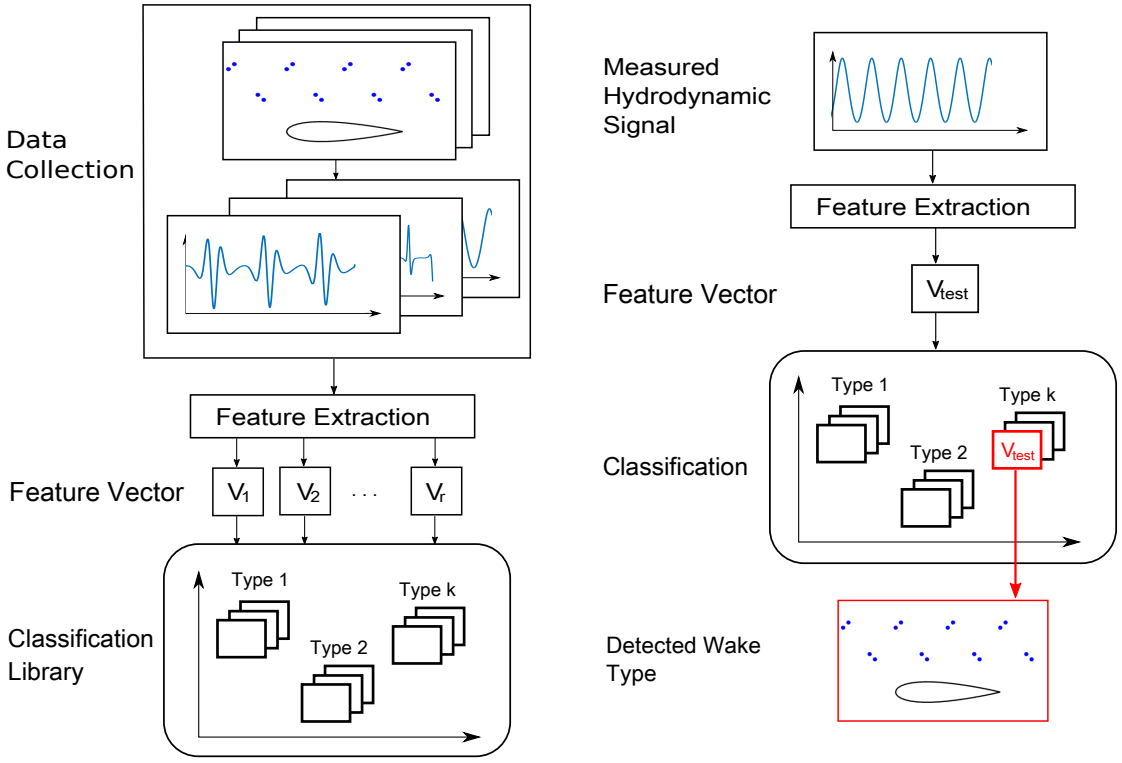

(a) Library construction **(b)** Wake Classification

Figure 1: The problem of wake classification utilizing hydrodynamic signals consists of two parts, i.e., the construction of classification library in (a) and the wake classification process in (b).[4]

The description of the wake classification protocol above is generally applicable, but was not demonstrated in the context of datastreams. The flexibility to handle datastreams is an important consideration to make wake detection and classification more relevant for real-time applications. In the remainder of this section, we show that the feature extraction stage of the wake detection protocol can be performed in a "streaming" fashion such that feature vectors can be extracted from online measurements. Further, the particular formulation here allows the wake detection protocol to be used in scenarios with time-varying/non-stationary environmental conditions. That is, if a nearby wake appears, changes form, then disappears, each of these events can be detected and classified accordingly.

A datastream can be viewed as an ever growing set of time-series data. Thus, direct application of a fast Fourier transform (FFT) would be problematic from a computational standpoint, since the length of the time-series data would be tending to infinity. Here, we will make use of short-time Fourier analysis[13] to obtain a sort of "streaming FFT" method that will allow for online feature extraction from a datastream. Here, rather than applying the FFT to a complete set of time-series data in post-processing, we make use of a sliding window approach (see Fig. 2). That is, only a short burst of sensor data is processed each time a feature vector is required by the wake detection protocol. Since the frequency content of the measured signal is not known *a priori*, the length of the sampling window may lead to spectral leakage due to signal truncation.[14] In order to overcome this issue, the data at the edges of the window can be "tapered" with a weighting function $w(j,\ell)$ centered at time index ℓ. However, this tapering approach will lead to the data at the edges of the window being ignored. To avoid this issue, as new bursts of data become available, the sliding window is shifted so as to capture this new data, but is done so in a manner that retains some overlap with previously processed data. Specifically, the sliding window selects data over the time interval $k(T_w - T_o) \leq t \leq k(T_w - T_o) + T_w$, where T_o is the overlap time, T_w is the window duration, and $k = 0, 1, 2, \ldots$ is the window index. Selecting an overlap of 50% to 75% of T_w typically yields favorable results.[14] In our study, data is sampled with a sampling period dt, and we take the time index for each sample in the window

to be $0 \leq n \leq N_w - 1$, where N_w is the total number of samples in the window. Further, we choose $w(j,\ell)$ to be a Hann function,[11,14]

$$w(j,\ell) = \begin{cases} \frac{1}{2}(1 - \cos(\frac{2\pi(j-\ell)}{N_w - 1}), & 0 \leq j \leq N_w - 1 \\ 0 & \text{otherwise.} \end{cases} \tag{1}$$

The Hann function guarantees that the data at the edges of a window will not lead to discontinuities due to the periodicity assumptions of the Fourier transformation. The latest burst of data is updated according to

$$g_i \leftarrow w(j,\ell)\left[g_i + w(j,\ell)g_{i-1}\right], \tag{2}$$

then the frequency-domain representation $\widehat{g}_i$ of the weighted signal can be computed via a standard FFT of g_i.

The power spectrum of the i^{th} window is calculated from $\widehat{g}_i$ for each window as,

$$P_i(\omega_\ell) = \langle \widehat{g}_i, \widehat{g}_i \rangle. \tag{3}$$

Further, defining T_s as the duration over which the window slides—corresponding to M total windows—the power spectrum of the signal over the full sliding duration T_s is given by,

$$P(\omega_\ell) = \frac{1}{M}\sum_{i=1}^{M} P_i(\omega_\ell). \tag{4}$$

Lastly, since we have used a weighting function $w(j,\ell)$ in the procedure, a modified power must be used to account for the associated rescalings. We arrive at the final power spectrum $\overline{P}(\omega_\ell)$ by imposing the condition that,[12]

$$\frac{1}{M}\sum_{i=1}^{M} {g_i}^2 = \sum_{\ell=-N}^{N-1} \overline{P}(\omega_\ell). \tag{5}$$

A graphical depiction of the sliding window algorithm is shown in Fig. 2. This method saves computational effort by performing the FFT over a relatively short window. The method can detect changes in the signal due to non-stationary effects and dynamic events. Lastly, by shortening the window length and overlap width, latency in the online feature extraction can be reduced while retaining an acceptable accuracy for later classification tasks. Further details of this point will be shown in Section IV.

III. Theoretical Modeling

In this section, introduce an ideal-flow model to simulate wake signatures on a fish-like body. To this end, we represent different wakes as a singly-periodic array of point vortices and by changing the number of point vortices in the base strip, 2S and 2P wakes can be modeled. A vortex panel method is applied to model a fish-like body. The hydrodynamic signatures imparted on the fish-like body by different wakes is simulated by combining these two models via a one-way coupling. The following sections summarize the main features of each of these models. For a detailed description, see our previous work.[4]

III.A. Point Vortex Modeling of Wake Dynamics

Consider N point vortices in a singly-periodic strip of length $L \in \mathbb{R}$ (see Fig. 3). The equations of motion for N point vortices are,

$$\frac{\mathrm{d}z_\alpha^*}{\mathrm{d}t} = \frac{1}{2Li}\sum_{\substack{\beta=1 \\ \beta\neq\alpha}}^{N} \Gamma_\beta \cot\left[\frac{\pi}{L}(z_\alpha - z_\beta)\right], \tag{6}$$

where $\Gamma_\beta \in \mathbb{R}$ denotes the strength of vortex β, and $z_\alpha(t) \in \mathbb{C}$ and $z_\beta(t) \in \mathbb{C}$ represent the complex position of vortex α and β, respectively. This expression governs the evolution of all vorticity in the singly-periodic

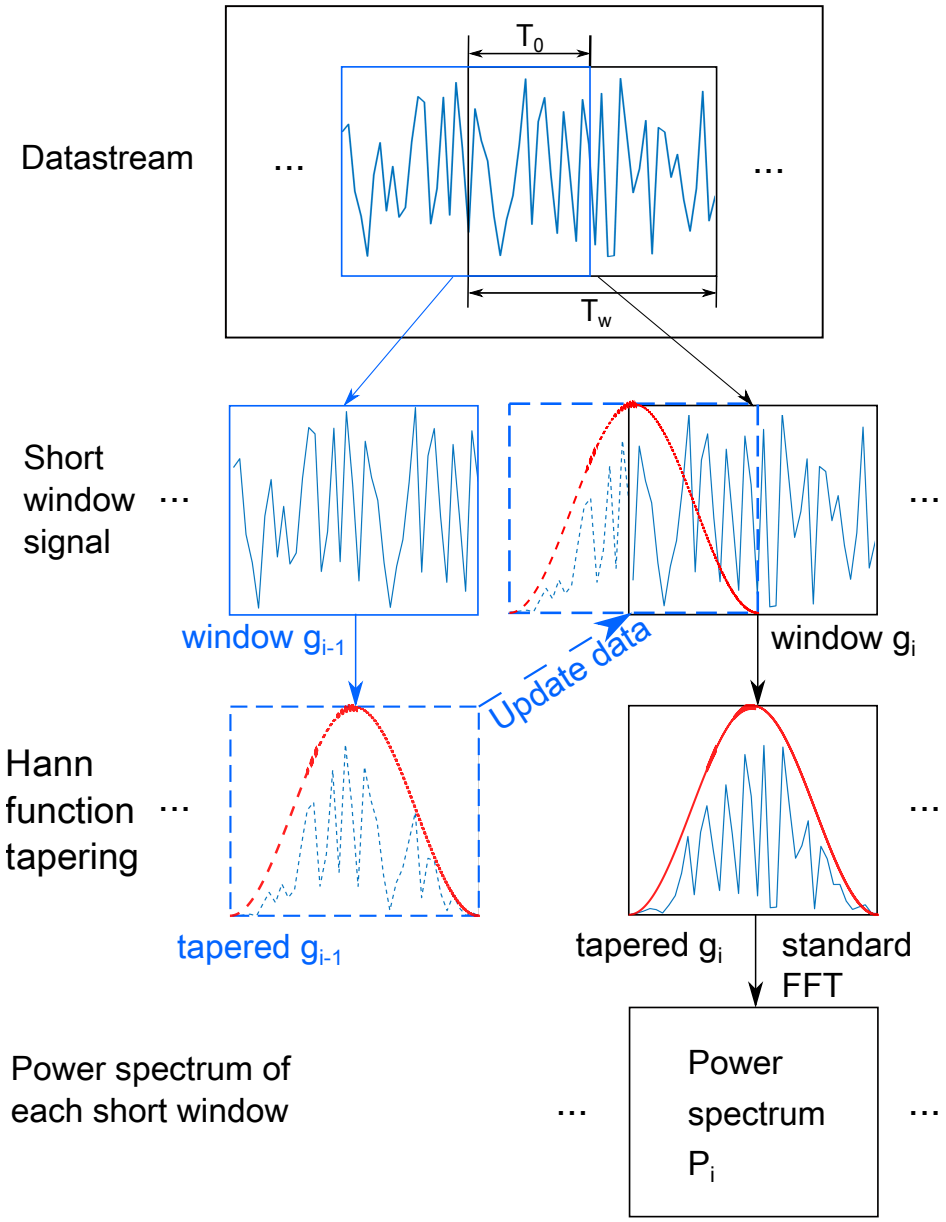

Figure 2: The window signal g_i is overlapped with the previous tapered window signal g_{i-1} for time T_o, then weighted with the Hann function. By performing a standard FFT on the now tapered g_i, we can obtain the power spectrum for the window signal. The process is repeated through the end of the full sliding duration T_s. The power spectrum over the full sliding duration T_s is determined by (5).

domain. Specifically, considering the wake is generated as a periodic shedding of vortices from a bluff body,[5]

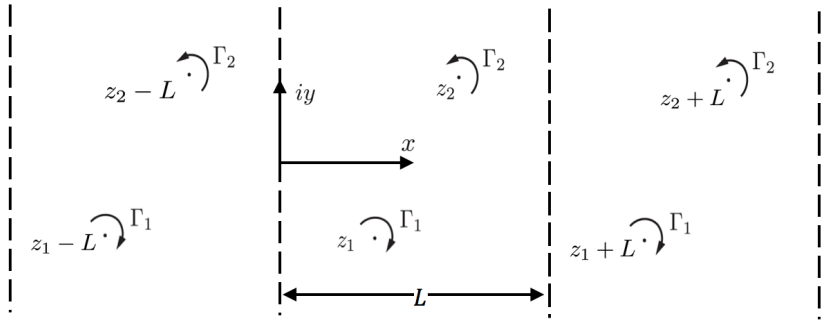

(a) Idealized 2S wake model ($N = 2$)

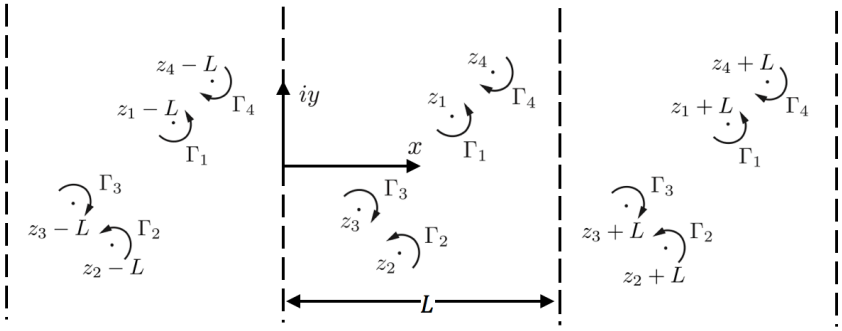

(b) Idealized 2P wake model ($N = 4$)

Figure 3: The evolution of point vortices on a singly-periodic strip is used to model the dynamics of different wakes. Here, three spatial periods are plotted for the point vortex models associated with (a) a 2S wake and (b) a 2P wake.

the sum of vortex strengths Γ_∞ is assumed to be zero for all time:

$$\Gamma_\infty = \sum_{\alpha=1}^{N} \Gamma_\alpha = 0. \tag{7}$$

In the case of a 2S wake with two single vortices shed per oscillation cycle (see Fig. 3a), it follows from $\Gamma_\infty = 0$ that the strengths of the two point vortices in each strip are equal and opposite (i.e., $\Gamma_1 = -\Gamma_2 = \Gamma$). The equations of motion for the 2S wake then reduce to

$$\frac{\mathrm{d}{z_1}^*}{\mathrm{d}t} = -\frac{\Gamma}{2Li} \cot\left[\frac{\pi}{L}(z_1 - z_2)\right], \tag{8}$$

$$\frac{\mathrm{d}{z_2}^*}{\mathrm{d}t} = \frac{\Gamma}{2Li} \cot\left[\frac{\pi}{L}(z_2 - z_1)\right]. \tag{9}$$

and the complex separation $(z_1 - z_2) = (\Delta x + i\Delta y)$ is a constant of motion, which implies that the motion of wake vortices will be parallel to the wake-axis. Two configurations can be achieved depending on the horizontal spacing Δx: (1) staggered vortices, and (2) aligned vortices.[4] In this study, we only focus on the staggered 2S configuration ($\Delta x = L/2, \Delta y = 0.28L$), since it corresponds to the von Kármán-type wakes that are commonly-observed behind bluff bodies and marine swimmers.

The dynamics of 2P wakes can also be modeled analogously, now setting $N = 4$ (see Fig. 3b). Following the works of Stremler and colleagues, we take the base vortex positions and strengths to be related as,[5–7]

$$\Gamma_3 = -\Gamma_1, \qquad \Gamma_4 = -\Gamma_2 \tag{10}$$

$$z_3 = z_1^* - \frac{L}{2}, \qquad z_4 = z_2^* + \frac{L}{2}. \tag{11}$$

Defining $S := \Gamma_1 + \Gamma_2$ and $\gamma := \Gamma_1/S$, it follows that the non-dimensional linear impulse for the base vortices

$\mathcal{Q} + i\mathcal{P} = (\pi/LS)\sum_{\alpha=1}^{N}\Gamma_\alpha z_\alpha$ reduces to

$$\mathcal{Q} = \frac{\pi}{2}(2\gamma - 1) \tag{12}$$

$$\mathcal{P} = \frac{2\pi}{L}\left[\gamma y_1 + (1-\gamma)y_2\right]. \tag{13}$$

Upon defining $Z := X + iY = \pi(z_1 - z_2)/L$ as the normalized separation between the first and second base-vortices, the equations of motion can be written in Hamiltonian form[5] as,

$$\mathcal{H} = \mathcal{H}(X, Y; \gamma, \mathcal{P}). \tag{14}$$

In this equation, the motion is parameterized by the strength ratio γ and the imaginary part of linear impulse $\mathcal{P}$ of the vortex pairs. These two parameters fix all possible dynamical regimes, while the initial vortex positions determine which among these is actually realized. For complete details and analysis of this dynamic wake model, see the works by Stremler and colleagues.[5,7]

III.A.1. 2P Wake regimes of interests

A complete analysis of the dynamics of the 2P wake model can be found in Basu and Stremler.[5] Depending on the parameters γ and $\mathcal{P}$, five distinct motion patterns can arise: orbiting, exchanging, scattering, passing, and mixed. These wake patterns can further be divided into dynamical sub-regimes based on separatrices in phase-space (see Fig. 4 for an example of the O_1 and O_2 orbiting sub-regimes).

Next, we discuss some of the representative sub-regimes, then explain how we determine the wakes of interest for assessing wake classification performance. The Hamiltonian level curves for $\gamma = \frac{3}{7}$ and $\mathcal{P} = -0.55$ are shown in Fig. 4. These level curves are associated with an exchanging wake(E_1), and two orbiting wakes (O_1 and O_2). The phase-space trajectories reveal that the motion patterns of these sub-regimes, which can be seen in physical space in tiles (b)–(d).

Both Fig. 4 and Fig. 5 show the representative 2P wake regimes. However, in Passing and Scattering wakes (see Fig. 5), the trajectories of vortex pairs begin to extend widely in the y direction based on their initial positions. In these terms, it is not proper to consider these cases in our study because they are unlikely to realized in practice. First, both the passing and scattering wakes occur under the special condition that $\gamma = 1/2$. Even if these wakes can arise in practice, they will leave a 2S-like signature on the swimmer's body: the fact that $\gamma = 1/2$ indicates that each of the vortex pairs will separate into a side-by-side configuration, and ultimately become two divided von Kármán-type configurations, as time progresses.

The last class of 2P vortex motion to be discussed here is the mixed 2P wake type. From Basu and Stremler's work and inspection of the phase-space trajectories,[5] this class of wake pattern appears in the region of the transition from orbiting to exchanging regimes, or from one type of orbiting wake to another. As discussed in Basu and Stremler, the mixed wake displays a combination of orbiting and exchanging motion behaviors. Inspection of the phase-portrait shows that the mixed regime evolves along trajectories adjacent to the boundaries with orbiting and exchanging regimes.[5] In this study, the mixed wakes will not be taken into consideration in classification based on features extracted from dynamics. According to the discussion above, our study only uses the simulated data from exchanging and orbiting wakes, since these two sub-regimes of 2P wakes are more likely to occur in practice.

III.B. Vortex Panel Modeling of Fish-Like Body

In this study, a fish-like body is modeled using a lumped vortex panel method. A summary of the model is given here; a full description can be found in Wang and Hemati.[4] A symmetric airfoil is represented by a set of n_{panel} vortex panels, with a point vortex placed at each panel's quarter-chord point (see Fig. 6. The strength of each vortex panel Γ^{panel} is initially unknown. The external wake and the uniform flow both impart a velocity at collocation points along the body (x_c, y_c), one at the three-quarter chord point of each panel To solve for the unknown strengths, the no-flow-through condition is imposed at each collocation point. The Kutta condition in our method is automatically satisfied due to the arrangement of panels and the nature of the lumped vortex panel method.

The influence of the external wake is give by,

$$U_{wake} = \sum_{\alpha=1}^{N} \frac{\Gamma_\alpha\left(-\sinh(\Delta y_\alpha),\ \sin(\Delta x_\alpha)\right)}{2L\left(\cosh(\Delta y_\alpha) - \cos(\Delta x_\alpha) + \epsilon\right)} \tag{15}$$

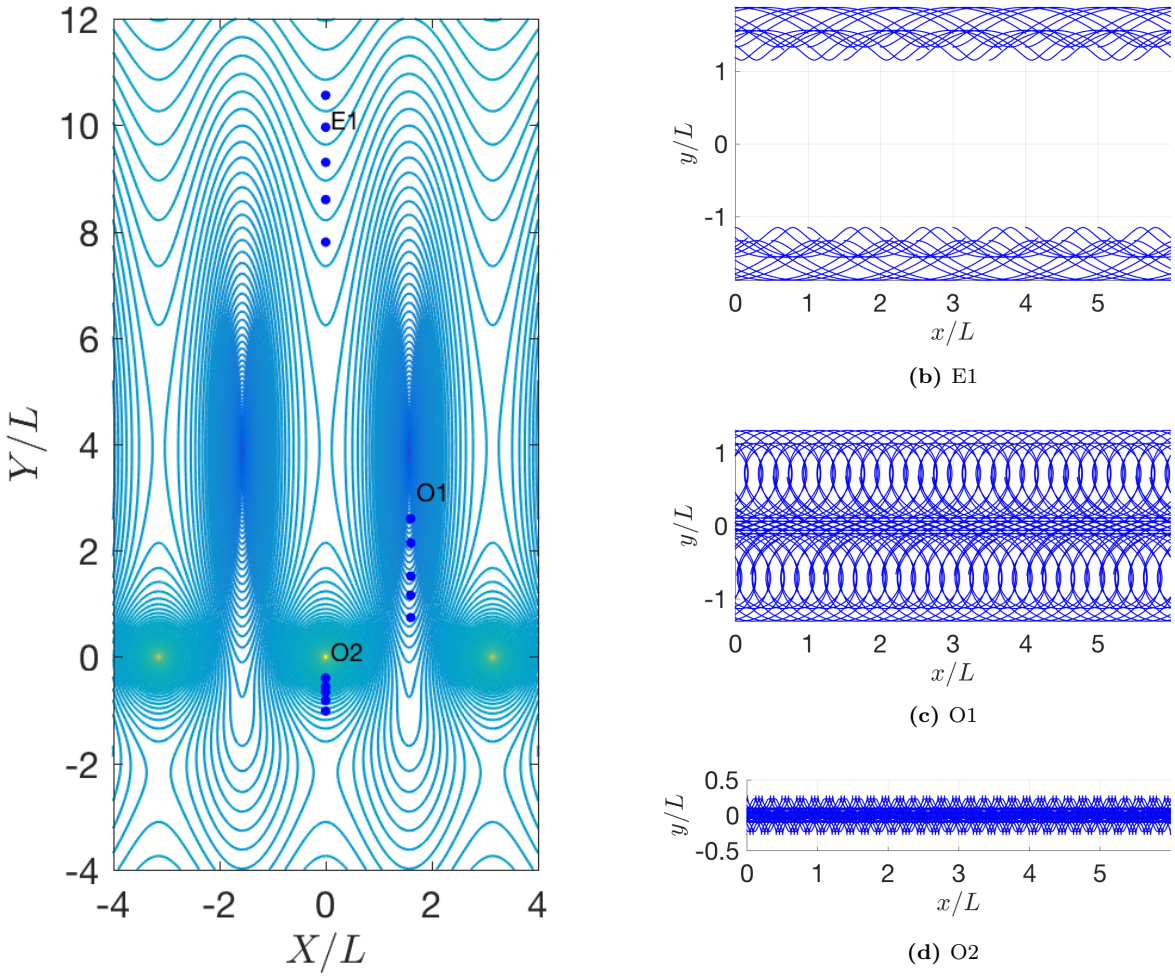

(a)

(b) E1

(c) O1

(d) O2

Figure 4: Level curves of $\mathcal{H}$ define trajectories with qualitatively different behaviors in phase-space (X, Y) and physical-space (x, y). (a) shows level curves of $\mathcal{H}$ corresponding to the 2P wake model with $\gamma = \frac{3}{7}$ and $\mathcal{P} = -0.55$. Three wake regimes are highlighted: $E1$, $O1$, and $O2$. The blue dots correspond to the particular initial conditions used to realize these classes of motion. Tiles (b)–(d) show sample trajectories of vortices in physical-space from each of these regimes.

where $\Delta x_\alpha = \frac{2\pi}{L}(x_c - x_\alpha)$, $\Delta y_\alpha = \frac{2\pi}{L}(y_c - y_\alpha)$, and ϵ is a regularization parameter that is used to ensure smoothness of solutions. Note the U_{wake} is a function of time since the induced velocity at each collocation point will change with respect to the evolution of the wake vortices.

In the remainder of the study, we focus on time-series measurements of local velocity at a fixed collocation point on the body surface. Let signal U' denotes the tangential velocity at this collocation point with the tangential component of the uniform flow velocity subtracted out.

III.C. Wake Signatures Measured with a Body-Mounted Velocity Sensor

The fish-like body is placed a lateral distance h away the wake. Fig. 6 shows a snapshot of this arrangement for a particular 2P wake. In this study, the hydrodynamic sensor measures U', the tangential component of local velocity with the contribution of the freestream subtracted. In our previous work, we found that the signal characteristics were relatively insensitive to sensor location.[4] Here, measurements of U' will be taken at the mid-chord $x/c = 0.5$ on the surface of the wake-side of the body; representative sensor signals for different wake types are shown in Section IV. In an effort to maintain objectivity in the assessment

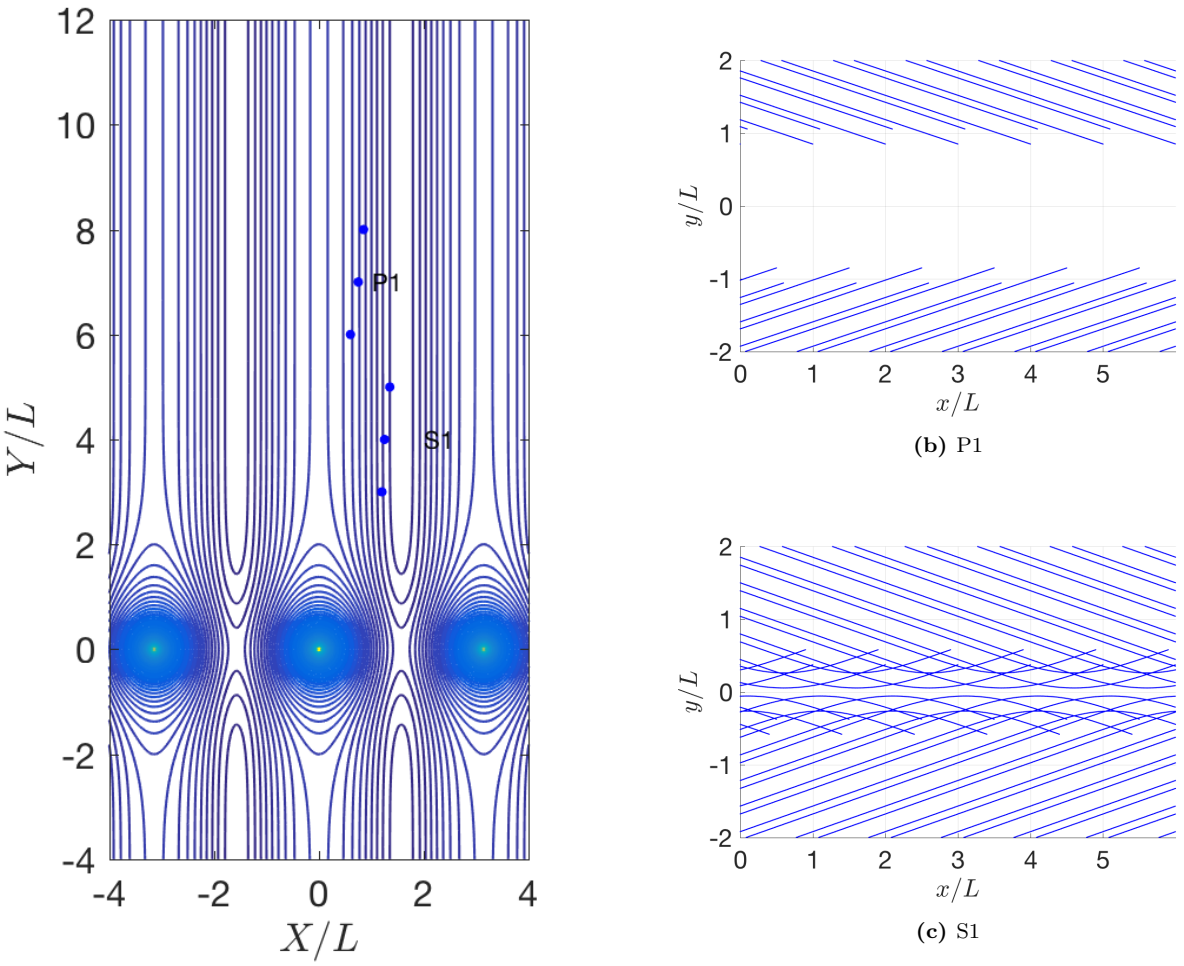

(a)

(b) P1

(c) S1

Figure 5: Representative trajectories for passing and scattering regimes. (a) shows level curves of $\mathcal{H}$ corresponding to the 2P wake model with $\gamma = \frac{1}{2}$ and $\mathcal{P} = -0.65$. Two wake regimes are highlighted: $P1$ and $S1$. The blue dots correspond to initial conditions used to realize these classes of motion. (b) and (c) show the expanding trajectories of vortices in passing and scattering 2P wakes.

of the wake classification study, we fix the closest lateral separation between a wake vortex and the body to be $h = 0.2L$. This is necessary since the lateral position of 2P wakes changes in time; by fixing the minimum lateral separation, the signal magnitude will remain comparable between wake realizations, and so the classification will primarily be based on the temporal signatures of the wakes and not on the relative magnitudes of the mean signals.

IV. Results: Wake Classification

In this study, a NACA 0020 airfoil with chord-length c is used to model the fish-like body. The airfoil is represented by a total of $n_{panel} = 40$ vortex panels. Sensor measurements are sampled uniformly with a convective time-step $dt = 0.01$. In all the results presented, the measured hydrodynamic signal U' at a collocation point corresponds to the tangential component of local velocity with the tangential component of the freestream removed. The U' measurements are taken at the $x/c = 0.5$ on the wake-side of the body. Representative signals of U' from various wake types are shown in Fig. 7. These signals reveal that different wakes impart distinct hydrodynamic signatures on the body, which permits these regimes to be distinguished from one another. In the next section, we discuss the specific feature vectors that can be extracted from

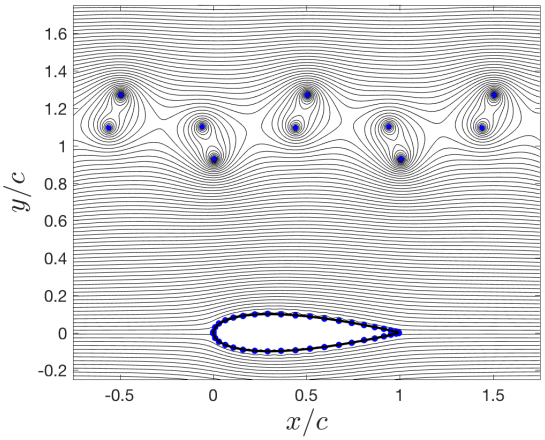

Figure 6: Model of a fish-like body with a nearby 2P wake.

these signals to perform classification using supervised learning techniques.

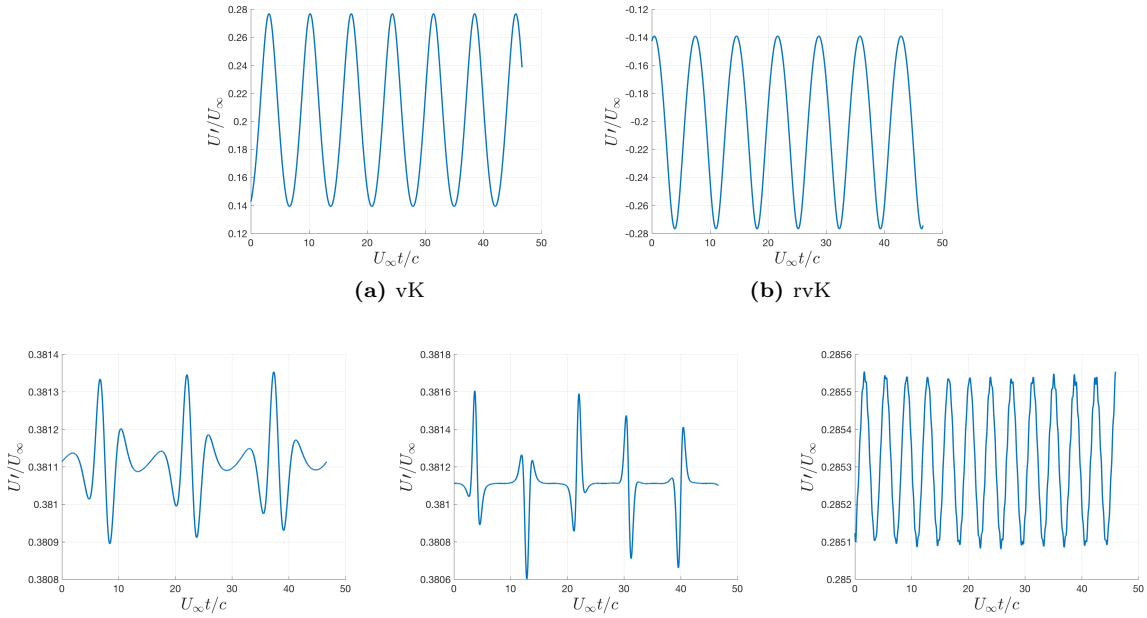

(a) vK **(b)** rvK

(c) E1 **(d)** O1 **(e)** O2

Figure 7: Sensor signals have notable qualitative differences between different wake regimes. The representative signals shown here correspond to (a) $\Gamma = 0.4$ (b) $\Gamma = -0.4$ and (c)–(e) $\gamma = 3/7$, $\mathcal{P} = -0.803$ with $\mathcal{H} = -0.2, 0.4$, and 0.13, respectively.

IV.A. Feature Extraction and Classification

The wake signatures from different wake types, shown in Fig. 7, have noticeable differences in frequency content, which can be clearly seen by frequency domain representations of these signals, as shown in blue in Fig. 8. Comparing the frequency domain signatures of various wake types leads to the choice of using the parameters (μ, a, σ) of a Gaussian bell curve fit to these frequency domain signatures as feature vectors for

classification,

$$F(x) = a \exp\left(-\frac{(x-\mu)^2}{2\sigma^2}\right). \tag{16}$$

An example of a fitted Gaussian bell curve is shown in Fig. 9. A feature vector for each wake realization i can then be defined using the parameters of the associated best-fit Gaussian bell curve:

$$V_i = (\mu_i, a_i, \sigma_i). \tag{17}$$

For library construction, feature vectors V_i are extracted from the complete dataset in a post-processing fashion. One such wake library for is shown in Fig. 10. Once a library of feature vectors is available, numerous alternative classification algorithms can be applied to determine the likelihood that the signature from an unknown wake belongs to a particular class of wakes stored in the library. Here, we make use of the relatively simple k-nearest-neighbor (KNN) algorithm. Note, in the present study we assign a wake label to each feature vector, assuming that we have prior knowledge of the wake types during the library construction stage. If the wake types were unknown at this point, unsupervised wake regime learning techniques could be used to assign these labels automatically.[8]

The short-time Fourier algorithm described in Section II can also be used to extract feature vectors V_i, now from datastreams in online applications. Here, we used an overlap percentage of 50%. Fig. 8 shows, in red, the frequency spectra and feature vectors for a fixed window $T_w = 0.16$ that slides over various durations T_s of the datastream, all reported in convective time units. Note that the blue curves in the same figure correspond to features extracted from a standard FFT of the full dataset. As one would expect, the online method converges to the batch result as sliding duration is increased, since only a single period of data is needed. However, as we will see, even when the classification library is constructed using the batch result and shorter sliding durations are used for online classification, classifier accuracy can still remain comparable to the longer sliding duration cases. Although applying the standard FFT to a shorter duration of data may yield comparable features as well, the short-time formulation has the added benefit of detecting changes in the environment through the use of sliding windows and weighting functions.

A graphical summary of the general wake classification framework is shown in Fig. 11.[4]

IV.B. Wake Classification Performance

In this section, we assess the performance of the wake detection and classification protocol described above. In addition to the wakes used to build-up the classification library, an additional set of unique wake realizations is used to determine the accuracy rate of the protocol via sample point testing. An example of this procedure for a single test point is shown in Fig. 12, with the test point marked with a black x and the $k = 7$ nearest-neighbors circled in red. Based on the labels of these $k = 7$ nearest-neighbors, a voting procedure is applied, and the type of the test wake is determined by the wake classifier. For performance assessment, we know the actual wake type of the test wake, so we compare the classifier result with the known type. This procedure is repeated for all test wakes, then the accuracy rate can be computed as the percentage of test wakes that were assigned correct labels by the wake classifier. Various algorithm parameter values can be modified, so their influence on performance can be determined. In our study, 50 test wakes are used in the performance assessment; each test wake is distinct from the wakes used to construct the classification library.

When the protocol is used in a post-processing capacity, the accuracy rate is above 95% in most cases (see Fig. 13) The number of nearest-neighbors k is varied between 3 and 11, and the number of elements in the library is varied from 30 to 150. The results of our study suggest that accuracy rate of the protocol degrades when the library is sparsely populated and the number of nearest-neighbors is large. It appears that accuracy rate is more sensitive to the richness of the library. For larger numbers of library entries, the accuracy rate is more or less constant with k.

Next, we consider accuracy rate for the online protocol, varying the sliding window duration T_s (see Fig. 14). The accuracy rate is relatively low for a short duration of sliding, but increases with T_s. This observation is consistent with our expectations based on analysis of the features in Fig. 8; the feature vectors determined online converge to feature vectors extracted from the full time-series data as T_s increases. However, even with the shortest waiting time considered, $T_s = 1.28$, the accuracy rate for most cases is 85%, indicating that the algorithm parameters can be tuned to improve other aspects of performance (e.g., latency), while balancing with accuracy.

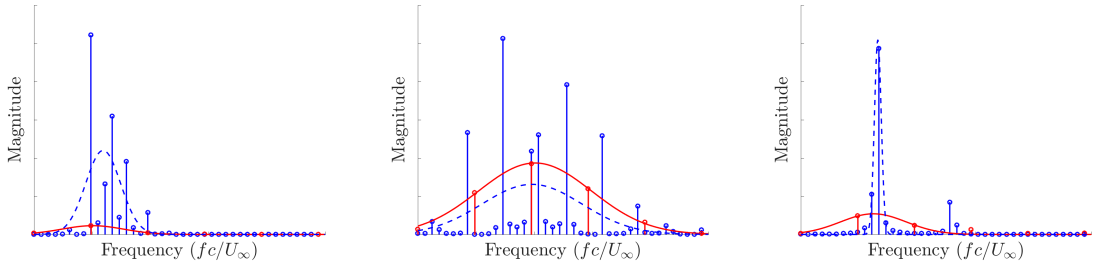

(a) E1 wake, $N_s = 128, T_s = 1.28$ **(e)** O1 wake, $N_s = 128, T_s = 1.28$ **(i)** O2 wake, $N_s = 128, T_s = 1.28$

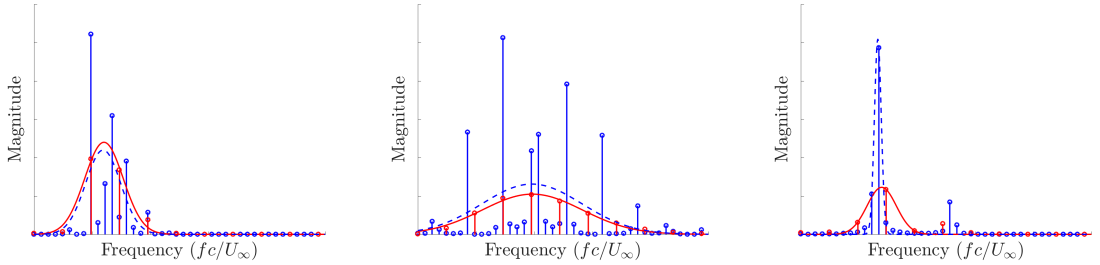

(b) E1 wake, $N_s = 512, T_s = 5.12$ **(f)** O1 wake, $N_s = 512, T_s = 5.12$ **(j)** O2 wake, $N_s = 512, T_s = 5.12$

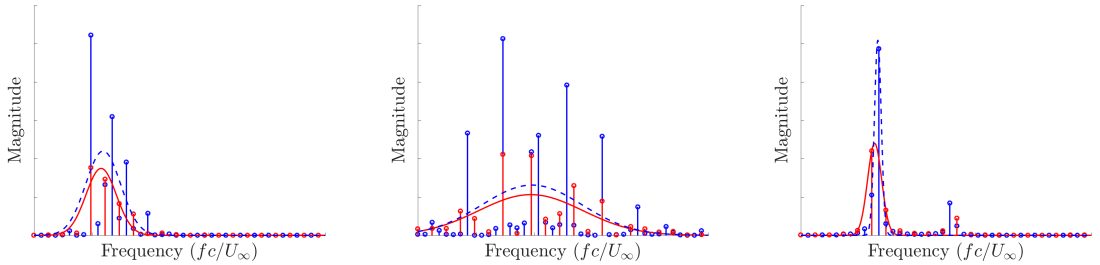

(c) E1 wake, $N_s = 2048, T_s = 20.48$ **(g)** O1 wake, $N_s = 2048, T_s = 20.48$ **(k)** O2 wake, $N_s = 2048, T_s = 20.48$

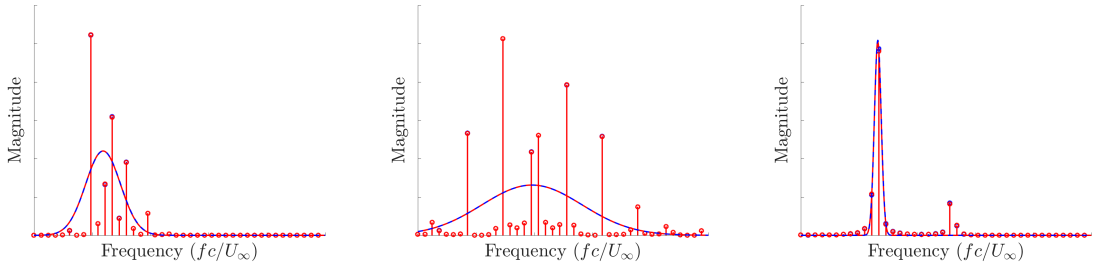

(d) E1 wake, $N_s = 8192, T_s = 81.92$ **(h)** O1 wake, $N_s = 8192, T_s = 81.92$ **(l)** O2 wake, $N_s = 8192, T_s = 81.92$

Figure 8: Comparison of the standard FFT (blue) with the sliding window approach (red). simulated data for different sub-regimes of 2P wakes. For the online method, the window duration is $T_w = 0.16$ which slides over various durations T_s as noted in the sub-captions. The stem plots correspond to frequency spectra, whereas bell curves correspond to the fitted features for classification.

Thus far, our performance studies have assumed perfect measurements without uncertainty. In practice, sensors will invariable yield uncertain measurements, so we assess the performance of the protocol in the context noisy signals. To model the measurement uncertainty, we add zero-mean normally distributed noise to the hydrodynamic signals. We vary the intensity of the synthetic noise to determine the sensitivity of the wake detection protocol to the level of noise. In this study, we quantify the noise intensity through signal-to-noise ratio, which we define as the ratio of the signal mean to the standard deviation of the sensor measurement. The performance assessment is then conducted for $SNR = 1, 3, 10, 30, 100$, where $SNR = 1$

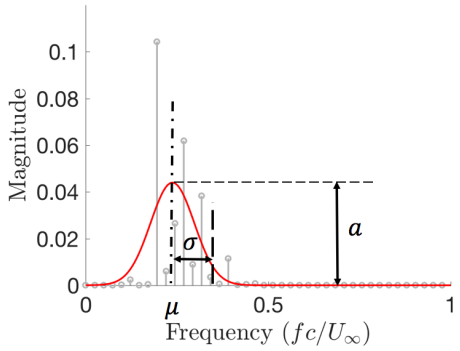

Figure 9: A Gaussian fit to the frequency signature yields a convenient, concise, and effective set of parameters (μ, a, σ) for use as a feature vector in the wake classification task. The parameters of the best fit Gaussian bell curve (drawn in red) concisely summarize this signature as a feature vector.

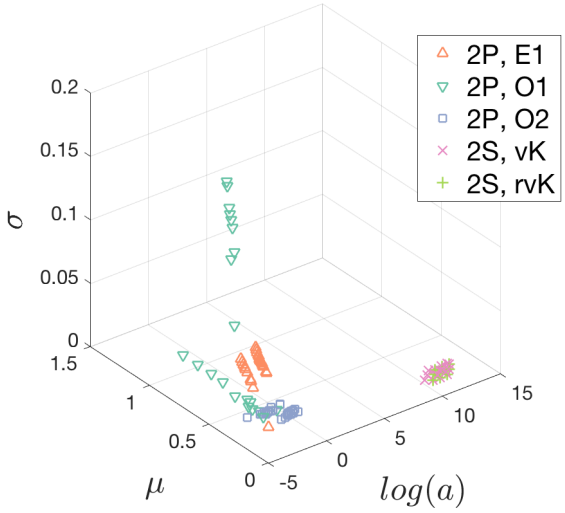

(a) Full Library

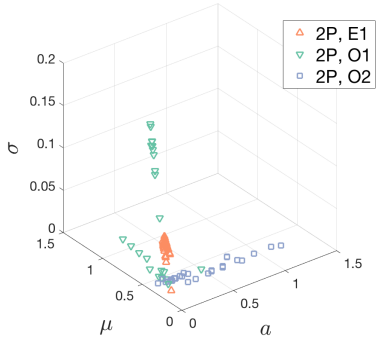

(b) 2P cluster in the library

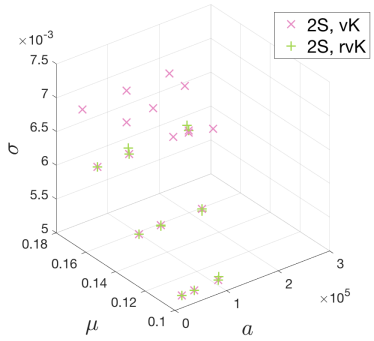

(c) 2S cluster in the library.

Figure 10: The wake classification library is built up in feature space with library entries from many wake types and regimes. In (a), an example of a classification library with a total of 150 entries is presented, equally distributed between the five regimes considered. The 2S and 2P wakes separate into distinct clusters here. A blown-up plot of the 2P and 2S clusters are shown in (b) and (c), respectively. Note that the 2P regimes are fairly well separated, whereas the 2S regimes are blended together.

is a high-noise intensity and $SNR = 100$ is a low-noise intensity. Representative noise-contaminated signals are shown in Fig. 15.

The accuracy rate of the wake detection protocol for various SNR and k values is presented in Fig. 16. The results here are based on a large library with 150 entries, which was found to be relatively insensitive to

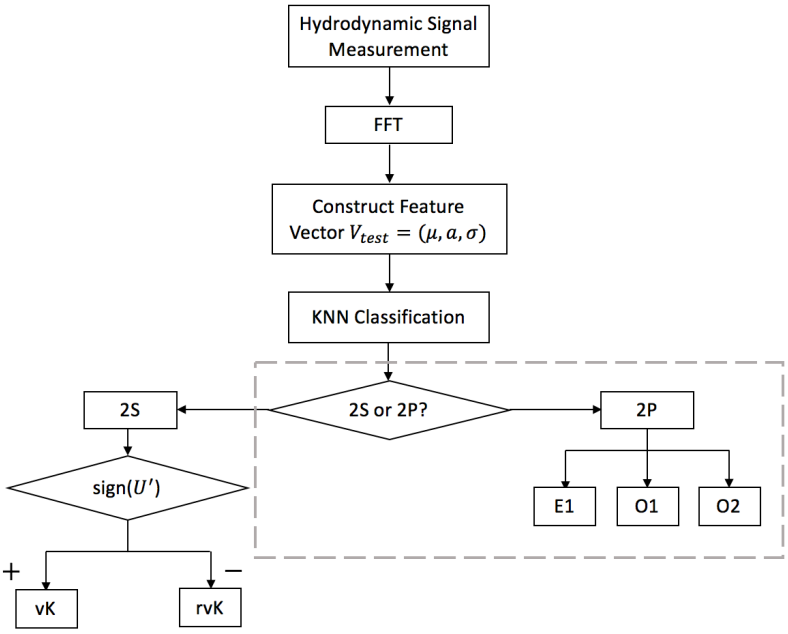

Figure 11: A graphical summary of the wake classification protocol. If a wake is determined to be 2P, then the classification is determined by closer inspection of the library. If a wake is determined to be 2S, the sign of the measurement signal U' can be used to determine whether the wake is a von Kármán vortex street or a reversed von Kármán vortex street.

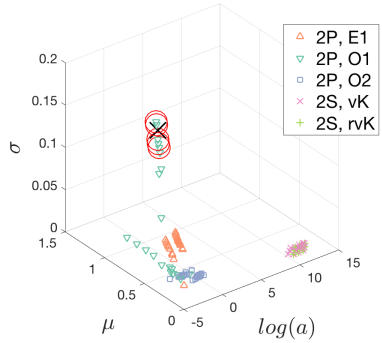

Figure 12: An unknown vortex wake has a feature located at x. The KNN method is used to compare this feature vector with the $k = 7$ nearest neighbors in the library to determine the most likely classification.

k in the context of perfect measurements (i.e., no measurement noise). Here, the noisy data are based on the same wake signals used in our performance assessment in the perfect measurement case shown in Fig. 13. For the highest-SNR (least-noisy) signals, accuracy rate is again relatively insensitive to k. However, as SNR is decreases (signals become noisier), accuracy rate for a given number of nearest-neighbors k. Further, the accuracy rate decreases with increasing k for $SNR \leq 10$. It appears that for high-noise environments, the protocol accuracy rate benefits from a smaller number of nearest-neighbors. Even for $SNR = 1$, the classification accuracy can reach $\geq 70\%$ with appropriate choice of k.

V. Discussion and Conclusions

In this study, we formulated an online protocol to detect and classify wakes from streams of hydrodynamic sensor signals. Short-time Fourier analysis techniques were used to extract features from short bursts of data,

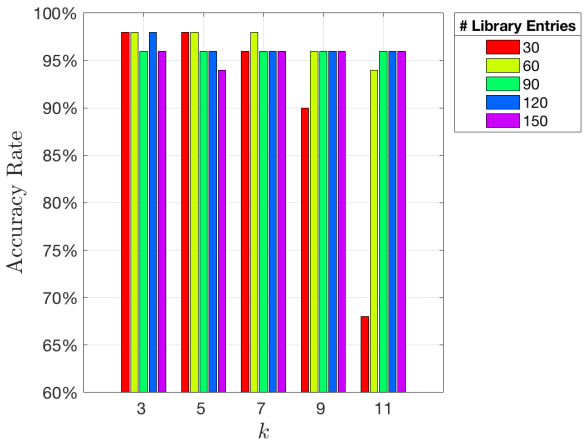

Figure 13: A study of accuracy rate as a function of algorithm parameters reveals that the wake detection protocol has good performance. The number of nearest neighbors k and the number of library entries are both varied in this study. Accuracy rate is measured based on 50 test signals from randomly generated wakes, and is defined as the number of correct classifications over the total number of test signals.

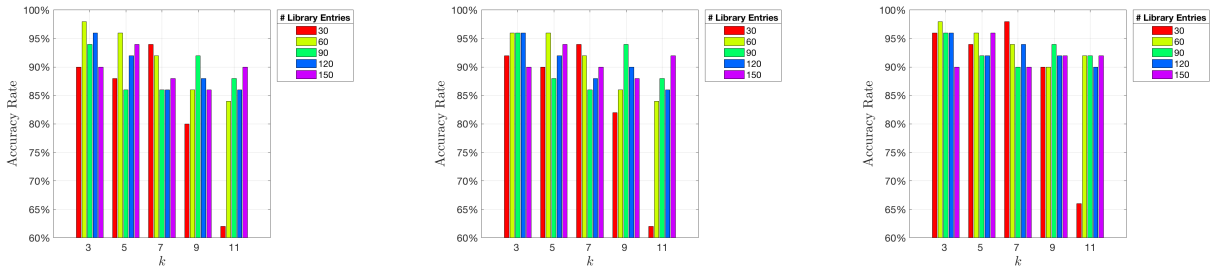

(a) $T_s = 1.28$ **(b)** $T_s = 5.12$ **(c)** $T_s = 20.48$

Figure 14: Accuracy Rate for streaming FFT with different input data lengths are shown with different value of k in KNN classification with various library entries. As the waiting time increases, i.e, T_s gets larger and larger, the accuracy performance will get better and closer to the classification accuracy utilizing an original FFT in Fig. 13.

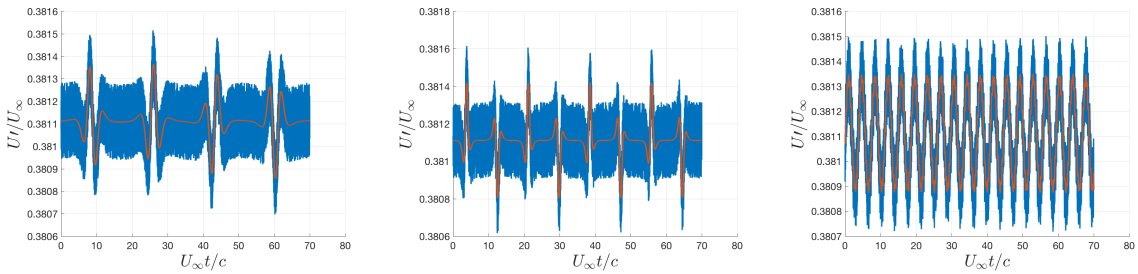

(a) Noisy E1 **(b)** Noisy O1 **(c)** Noisy O2

Figure 15: Representative wake signatures with $SNR = 3$. Signatures are generated by 2P wakes with $\gamma = 3/7$, $\mathcal{P} = -0.803$ and $\mathcal{H} = -0.2, 0.4$, and 0.13, respectively. The red curves are the original signals, and the blue curves are the noise-corrupted signals.

which were then compared with entries in a wake library for classification. The protocol was demonstrated on an ideal-flow model with dynamic wake evolution. Tangential velocity signals from a single point sensor

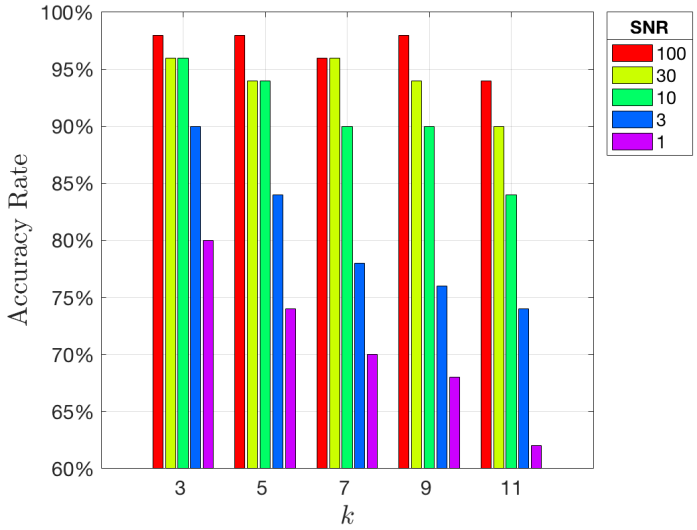

Figure 16: Accuracy rate for 50 noisy test data with different SNR values. The library has 150 entries.

on a body were sufficient for distinguishing between various wake types. The online protocol achieved an accuracy rate of 95% in most cases where measurement noise was not considered.

The results of the present study serve as a proof-of-concept demonstration for online wake detection and classification, moving such methods closer to practical use. An important contribution of this investigation is the ability to accommodate datastreams in the classification protocol. The approach taken can be used to detect changes in non-stationary/time-varying environments, owing to the nature of the sliding windows and weighting schemes employed in the formulation of the online classification algorithm. We found that the protocol could be tuned to balance accuracy rate with latency. When the waiting time was short, the accuracy rate was lower; however, by increasing the waiting time, accuracy rate was increased. Overall performance improved with a sufficiently rich classification library. The number of nearest-neighbors k could also be used as a tuning parameter to improve performance; however, in the context of noisy measurement signals, the classification accuracy rate was found to decrease with decreasing SNR, so such tuning may not be available in the context of low-SNR. That said, it was found that designing the protocol with fewer nearest-neighbors k for classification would maximize accuracy for $SNR \leq 10$, with accuracy rates $\geq 80\%$ possible.

An inherent performance challenge we observed was poor performance in distinguishing between wakes with evolutions near regime boundaries. In particular, mixed 2P wakes were difficult to distinguish from adjacent regimes. We found that constructing the classification library with mixed 2P wakes included would degrade overall classification accuracy. This suggests that wake detection for the mixed wake regimes may need special consideration. As such, the mixed 2P wakes were excluded in library construction for all the results considered here. Testing sample wakes from mixed regimes were not examined in the analysis of the library performance.

The approach presented here can be extended to synthesize measurements from distributed sensors. A feature vector based on the spatiotemporal character of a wake's signature is likely to be needed for improved reliability and performance, both in the context of noisy measurements and other complicating factors. In future work, we plan to extend the framework to accommodate factors such as relative positioning and alignment of the body and the wake.

The results presented here suggest that it may be possible to extend the online wake detection approach to more practical systems. Certainly, our findings can provide guidance for improving flow sensing capabilities in human-engineered systems.

References

[1]Liao, J.C., Beal, D.N., Lauder, G.V., and Triantafyllou, M.S., "Fish Exploiting Vortices Decrease Muscle Activity," *Science*, Vol.302(5650), 2003, pp 1566-1569

[2]Marras,S., Killen,S.S., Lindström, J., McKenzie, D.J., Steffensen, J.F., and Domenici, P., "Fish Swimming in Schools Save Energy regardless of Their Spatial Position," *Behavioral Ecology and Sociobiology*, Vol. 69(2), 2015, pp. 219-226.

[3]Zhang, F., Lagor, F.D., Lei, H., Tan,X., and Paley, D.A., "Robotic Fish: Flow-relative Control Behaviors Using Distributed Flow Sensing," *Mechanical Engineering*, Vol. 138(3), 2016, pp. 2-5.

[4]Wang, M. and Hemati, M.S., "Detecting exotic wakes with hydrodynamic sensors," pre-print arXiv:1711.10576, 2017.

[5]Basu, S. and Stremler, M. A., "On the motion of two point vortex pairs with glide-reflective symmetry in a periodic strip", *Physics of Fluids*, Vol. 27(10), No. 103603, 2015.

[6]Stremler, M. A., Salmanzadeh, A., Basu, S. and Williamson, C. H., "A mathematical model of 2P and 2C vortex wakes", *Journal of Fluids and Structures*, Vol. 27(5), 2011, pp. 774–783.

[7]Stremler, M.A. and Basu, S., "On point vortex models of exotic bluff body wakes," *Fluid Dynamics Research*, Vol. 46(6), No.061410, 2014.

[8]Hemati, M.S.,"Learning Wake Regimes from snapshot Data", *46th AIAA Fluid Dynamics Conference*, 2016, pp.3781.

[9]Bishop, C. M. "Pattern Recognition and Machine Learning", *Springer*, 2006.

[10]Tan, P.N., Steinbach, M. and Kumar,V., "Introduction to Data Mining", 2006.

[11]Grandke, T. ,"Interpolation algorithms for discrete Fourier transforms of weighted signals",*IEEE transactions on instrumentation and measurement*, Vol. 32(2), 1983, pp.350-355.

[12]Choi, H. and Moin, P., "On the spacetime characteristics of wallpressure fluctuations", *Physics of Fluids A: Fluid Dynamics*, Vol. 2(8), 1990, pp.1450-1460.

[13]Allen, J.B. and Rabiner, L.R., "A Unified Approach to Short-Time Fourier Analysis and Synthesis",*Proceedings of the IEEE*, Vol. 65(11), 1977, pp.1558-1564.

[14]Harris, F.J., "On the Use of Windows for Harmonic Analysis with the Discrete Fourier Transform", *Proceedings of the IEEE*, Vol. 66(1), 1978, pp.51-83.